Comparison of structural heterogeneity in Zr- and Pd-based metallic glasses

Running header: Structural heterogeneity based on a dynamic mechanical analysis

Hao Wang[1,a)], Sheng-Li Zhu[2], Zhen-duo Cui[2]

[1] *Institute for Materials Research, Tohoku University, Sendai, 980-8577, Japan*

[2] *School of Materials Science and Engineering, Tianjin University, Tianjin, 300350, China*

Author to whom correspondence should be addressed.
Electronic mail: a) hao.wang.e4@tohoku.ac.jp

Abstract: Metallic glasses (MGs) are known to exhibit a nanoscale heterogeneous structure that consists of a weakly bonded region (WBR) and a strongly bonded region (SBR), but its characterization is not yet fully understood. This study investigates the structural heterogeneity (SH) of Zr- and Pd-based MGs using a dynamic viscoelastic model. Volume fraction (V) and elastic modulus (E_c) are independently derived from the model to characterize each region. In addition, the SH is evaluated using $\chi = VE_{c,WBR}/VE_{c,total}$. As a result, the strong Zr-based MG is estimated to own approximately 28% of V_{WBR}, approximately 87% of $E_{c,WBR}/E_{c,SBR}$, and χ~0.241. On the other hand, the fragile Pd-based MG is estimated to own approximately 26% of V_{WBR}, approximately 70% of $E_{c,WBR}/E_{c,SBR}$, and χ~0.208. Furthermore, a comparison of χ, fragility (m), and Poisson's ratio (v) shows that as χ increases, m decreases and v increases. Notably, the diversification of constituent elements is inversely related to χ, m, and v in the Zr- and Pd-based MGs. Thus, the existing understanding of the SH inherent in MGs is updated using the constructed dynamic viscoelastic model in this study.

1. Introduction

Metallic glasses (MGs) are of interest in materials science and condensed matter physics owing to their unique microstructures and mechanical and functional properties. In particular, they provide a simple and effective system for studying relaxation and related problems in glass science [1–4]. The relaxation-property relationship allows for the control of mechanical properties and design of new MGs with superior properties. Therefore, a proposal for a relaxation perspective is needed to understand MGs.

MGs with amorphous atomic structures are obtained by quenching and solidifying from a liquid phase at a certain critical cooling rate. They have local structures with an atomic arrangement lacking long-period regularity [1–4]. The higher the cooling rate, the more disordered and thermodynamically metastable the structure produced. Owing to their random long-range atomic structures, MGs evolve extremely slowly, reaching a more stable equilibrium state in a steep and tortuous energy regime at room temperature [1–4].

MGs have various relaxation modes, such as α-, slow β (sβ)-, and fast β (fβ)-relaxation [5–7]. As the α-relaxation disappears below glass transition temperature T_g, the sβ- and fβ-relaxations—which continue to occur below T_g—are the principal sources of the dynamics in the glassy state. Moreover, they are of practical significance to many properties of glassy solids [8–11]. The α-relaxation features are attributed to the reorganization of metastable clusters in supercooled liquids, as a large-scale irreversible rearrangement of atoms, and is associated with dynamic glass transition and viscous flow behavior. [12] Subsequently, the sβ-relaxation process is attributed to locally reversible atomic motion and plastic deformation. [5,6] Finally, the fβ-relaxation process is estimated as rattling motion of atoms in cages. [5,6] The relationship between relaxation modes and structural heterogeneity (SH) [13] have been discussed not only primarily from microscopic aspects [9,12,14–21] but also macroscopic aspects [3,4,7, 22]. The certain is that the sβ-relaxation is associated with the unrelaxed structures produced by rapid cooling, which are proposed to indicate SH. Particularly, Ichitsubo *et al.* [21] use inelastic X-ray scattering to experimentally verify that MGs have a nanoscale heterogeneous structure composed of a weakly bonded region (WBR) and a strongly bonded region (SBR). Moreover, the correlation length (ξ) of the WBR involved in the heterogeneous structure of $Zr_{65}Cu_{17.5}Ni_{10}Al_{7.5}$ and $Pd_{42.5}Ni_{7.5}Cu_{30}P_{20}$ MGs is investigated.

In our previous studies, we investigate the dynamic relaxation behavior of a $Pd_{42.5}Ni_{7.5}Cu_{30}P_{20}$ MG [5,6] at low temperatures (173 K) up to the glass transition temperature (563 K ≈ $0.98T_g$). Further, we use the obtained frequency-dependent curve to draw a master curve to identify the presence of fβ-relaxation as well as the activation energy of sβ- and α-relaxations and their distribution. However, the elastic modulus (E_c) and volume fraction (V) associated with these relaxation modes and SH proposed by Ichitsubo *et al.* [21] have not yet been derived.

To this end, this study analyzes the characterized relaxation modes based on the proposed intrinsic nanoscale heterogeneity concept for Zr- and Pd-based MGs. Subsequently, we compare the MGs in the assessment of SH based on dynamic relaxation analysis.

2. Experiments

A $Pd_{40}Ni_{40}P_{20}$ (PNP, T_g = 575 K [23]) MG matrix alloy is produced using the B_2O_3 flux method. We place a mixture of B_2O_3, Pd (99.5 mass%), Ni (99.99 mass%), Cu (99.99 mass%), and P (99.9999 mass%) in a quartz tube and melted the mixture under inert Ar gas in a resistance-heating furnace. $Zr_{50}Cu_{50}$ (ZC, T_g = 673 K [24]), $Zr_{50}Cu_{40}Al_{10}$ (ZCA, T_g = 693 K [25], and $Zr_{55}Cu_{30}Ni_5Al_{10}$ (ZNCA, T_g = 683 K [26]) are prepared by arc melting in an Ar gas atmosphere. A mother alloy is pulverized and fabricated into ribbon-shaped samples using a single-rolled quenching device. The samples are cut into pieces with a thickness, width, and length of 30 μm, 2 mm, and 30 mm, respectively. The fabrication method for the $Pd_{42.5}Ni_{7.5}Cu_{30}P_{20}$ (PNCP) MG is described in [5,6]. The relaxation behavior of the MG is measured via a forced vibration method using a dynamic viscoelasticity measuring device (RSA-G2, TA Instruments, USA) in an ambient atmosphere. The MG is placed vertically, and the response stress is measured at the upper edge while tensile strain is applied to the lower edge. The oscillatory strain is 0.2% owing to the elastic limit, and the distance between gauge points is approximately 10 mm. Isothermal frequency dispersion measurements are conducted from 323 to 718 K. Quasi-static tensile creep tests are conducted by thermomechanical analysis (TMA, Q400, TA Instruments Inc., USA) in a tensile mode with a melt-spun ribbon at a heating rate of 0.083 K/s from room temperature to T_g with constantly applied stresses of 12 and 100 MPa in an air atmosphere. The fitting model is referred to in refs. 5 and 6 [5,6].

3. Results and Discussions

Previously, we develop a dynamic viscoelastic model based on the Maxwell model associated with structural relaxation. We assume that fβ-relaxation originates from the rattling motion of atoms occurring in cages in both the SBR and WBR; the sβ-relaxation originates from α-relaxation in the WBR, which is actually reduced to be of almost single atomic diffusion because the region is too thin to have enough atoms for the cooperative motion for α-relaxation; and α-relaxation in the SBR is the macroscopically observed α-relaxation. Firstly, we use the model in elastic moduli mode to quantitatively analyze the isothermal dynamic mechanical properties of elastic moduli for PNCP MG, as follows [5]:

$$E' = \sum_{i=\alpha,s\beta,f\beta} V_i E_{c,i} \frac{\left(\omega\lambda_{c,i}\right)^{2\beta_{kww,i}}}{1+\left(\omega\lambda_{c,i}\right)^{2\beta_{kww,i}}}, \quad (1a)$$

and

$$E'' = \sum_{i=\alpha,s\beta,f\beta} V_i E_{c,i} \frac{(\omega\lambda_{c,i})^{\beta_{kww,i}}}{1+(\omega\lambda_{c,i})^{2\beta_{kww,i}}}, \quad (1b)$$

where E', E'', ω, λ_c, and β_{KWW} are the storage modulus, loss modulus, angular frequency, characteristic relaxation time, and Korausch-Williams-Watts (KWW) stretched exponent, respectively. Moreover, according to the time-temperature superposition rule, a master curve is constructed by shifting the separately measured isothermal E', and E''. Assuming an Arrhenius-type thermal activation for a relaxation mode [5],

$$\omega_p = \omega_0^n \exp\left(-\frac{nQ}{kT}\right), \quad (2)$$

where ω_p, ω_0, Q, k, and T are the peak angular frequency, preexponential factor, activation energy, Boltzmann constant, and temperature, respectively. In particular, we assume n nearly-identical processes cooperatively form a single process (the Debye frequency of ~14). Thus, for an unreasonably high value of ω_0, the process is estimated from derived Q/n. For example, for α-relaxation, Q = 7.98 eV and $\omega_0 = 5.1 \times 10^{68}$ rad s^{-1} gave Q = 7.98/(68/14) = 1.6 eV. This value corresponds to the magnitude of single atom diffusion, *e.g.*, 1.41 eV for P diffusion in Cu and 2.36 eV for Pd diffusion in Cu. [27] Thus, glass transition in the present case can be qualitatively understood to originate from the five-time cooperative motion of single atom diffusion. Similarly, sβ-relaxation in the PNCP MG is estimated to be monatomic diffusion. Additionally, fβ-relaxation is estimated as the rattling motion of atom(s) in a relatively loose binding condition within a cage by relatively tightly bound conditional atoms. However, a larger activation energy region (low-frequency side) of the fβ-relaxation distribution, which is associated with the rattling motion of atoms in cages, is measured in this test.

Secondly, we use the model in complex compliance (J^*) form to quantitatively analyze the isochronal quasi-static mechanical properties of creep compliance [6], as follows,

$$|J^*| = \sum_{i=\alpha,s\beta,f\beta} \frac{v_i^2}{\left[(v_i E_i')^2 + \left(v_i E_i''\right)^2\right]^{\frac{1}{2}}}. \quad (3)$$

According to Chen [28], the relaxation time (λ, inverse of ω) of α-relaxation with activation energy Q_m observed at temperature T_m during the kinetics with a heating rate of a = 0.33 K/s is calculated using eq. (4):

$$\lambda = \frac{1}{\omega} = \frac{kT_m^2}{Q_m a}. \quad (4)$$

Thereafter, V, E_c, and VE_c are estimated independently. Consequently, V, E_c, and VE_c for the α- (SBR) and sβ- (WBR) relaxations in the PNCP MG are estimated to be 0.74, 105, and 71 GPa; and 0.26, 84, and 21 GPa, respectively.

In this study, we similarly use the dynamic viscoelastic model to analyze the isothermal dynamic mechanical properties of elastic moduli and isochronal quasi-static mechanical properties of creep compliance for ZC, ZCS, ZCNA, and PNP MGs, as shown in figs. 1 and 2, respectively. The fitting parameters are listed in Tables 1 and 2. For these MGs, the α-relaxation peak is prominent while the sβ-relaxation exhibits as excess wing type rather than peak shape, as shown in fig. 1. Conversely, the sβ-relaxation for the PNCP MG exhibits a shoulder type in ref. 6 [6]. In Pd-based MG, it is known that the shape of the sβ-relaxation changes from excess wing to shoulder type with decreased Ni content. [29] Notably, the α- and sβ-relaxations in the ZC, ZCS, and ZCNA MGs are estimated as three atomic cooperative motions and monatomic diffusion, respectively. Here, the Q values for the α- and sβ-relaxations in ZC and ZCS are underestimated comparing with the Q values in ZCNA. Subsequently, the α- and sβ-relaxations in the PNP MG are estimated as four atomic cooperative motions and monatomic diffusion, respectively. Thus, from the fitting isothermal frequency dispersion of the elastic moduli, the peak of the α-relaxation is clearly identified, whereas the peak of the sβ- and fβ-relaxations are evident because the sβ-relaxation exhibits as excess wing type and the fβ-relaxation can only capture a slight trend on the low-frequency side in this experiment. Figure 2 shows the measured and fitted isochronal temperature (normalized by T_g) dispersion of the tensile creep compliance for the ZC, ZCS, ZCNA, and PNP MGs. From the slope change on the J^*, for instance, there are three slopes—above 1.0, below 0.8, and intermediate—in PNP MG, as shown in fig. 2(d). Those slopes represent the contribution of each relaxation. This is also evident for all other MGs. Moreover, V, E_c, and VE_c for α-SBR and sβ-WBR relaxations in the ZC, ZCS, and ZCNA MGs are estimated to be 0.29, 70, and 20 GPa; 0.3, 67, and 20 GPa; and 0.28, 73, and 21 GPa, respectively. Moreover, V, E_c, and VE_c for α-SBR and sβ-WBR relaxations in the PNP MGs are estimated to be 0.68, 89, and 60 GPa; and 0.33, 62, and 20 GPa, respectively.

Ichitsubo *et al.* [21] investigate ξ of the WBR involved in the heterogeneous structure of MGs, which is approximately 1 nm for a $Zr_{65}Cu_{17.5}Ni_{10}Al_{7.5}$ MG and approximately 4 nm for a PNCP MG. By using this result, they construct a schematic of the SH of the nanoscale network structure inherent in the PNCP MG by considering that there exists an approximately 1-nm length of the WBR, which is the site of sβ-relaxation, and a stronger bonding with a higher E_c and activation energy of the SBR, which is the site of α-relaxation. If the sβ-relaxation in the WBR around the SBR is not activated, the constraint

caused by the WBR will hinder multi-atom cooperative motion in the SBR. Subsequently, when the sβ-relaxation is activated by thermal activation, the constraint around the SBR is released. Moreover, cooperative motion of multiple atoms in the SBR, that is, α-relaxation, occurs. Because the excess wing is considered to be the same as the sβ-relaxation, as shown by Ngai *et al.* [30], the ZCNA MG is also considered to be formed by the SBR and WBR. This is consistent with the quantitative interpretation of various behaviors, assuming that the sum of V_α and $V_{s\beta}$ is approximately 1, as reported in previous studies [5,6]. However, the fβ-relaxation is the rattling of atoms trapped in cages of tightly bound atoms, which cannot form strong bonds with their surroundings, and occurs in both the SBR and WBR regions.

Ichitsubo *et al.* [21] show that a strong Zr-based MG with small fragility (m) has low SH and a small V_{WBR}. Meanwhile, a fragile Pd-based MG with a large m has a high SH and a large V_{WBR}. Assuming that $E_{c,WBR}$ and $E_{c,SBR}$ are similar, an MG with a small V_{WBR} will have a low SH, and an MG with a large V_{WBR} will have a high SH. In this study, estimating V and E_c for the WBR and SBR enables us to discuss SH in more detail. However, each value is independent and the degree of SH cannot be evaluated. Therefore, we evaluate SH from the contributions of both V and E_c as the intensity VE_c of the region. In other words, the degree of SH is evaluated using the strength ratio of the WBR to the overall strength, $\chi = VE_{c,WBR}/VE_{c,total}$. Herein, the overall intensity $VE_{c,total}$ is equivalent to the sum of VE_c for α-, sβ-, and fβ-relaxations. Considering the distribution of χ, when the value is close to 0, the V and E_c of the WBR are small, and the SBR becomes dominant, resulting in a decrease in SH. However, when χ is close to 1, the V and E_c of the WBR are large, and the WBR is dominant, resulting in a decrease in SH. In other words, when χ is 0.5, the difference between the WBR and SBR becomes most noticeable, which can be interpreted as high SH. Therefore, by comparing the magnitude of χ derived in this study, the degree of SH of various MGs can be determined.

Regarding the parameters for the ZC, ZCA, and ZCNA MGs in Table 2, VE_c, V, and E_c are relatively unchanged. However, χ exhibits a clear increasing trend. In other words, the increase in χ for the Zr-based MGs indicates that SH increases as the number of constituent elements increases. Similarly, regarding the parameters for the PNP and PNCP MGs in Table 2, χ exhibits a noticeable decreasing trend; that is, the SH for the Pd-based MGs decreases as the number of constituent elements increases. Moreover, these Zr- and Pd-based MGs exhibit high glass-forming ability as they are multi-component. Therefore, the SH of the glassy structure and the expansion of the glass-forming ability are assumed to be related.

Comparing the SH of the ZCNA and PNCP MGs, the χ values of these alloys are 0.241 and 0.208, respectively, indicating that ZCNA has a relatively low SH. Therefore, we summarize these characteristics as follows, and as shown in fig. 3:

1. ZCNA: $E_{c,WBR}/E_{c,SBR}$ is approximately 87%; approximately a 1-nm WBR is present at approximately 28vol%; and the SH is χ~0.241.
2. PNCP: $E_{c,WBR}/E_{c,SBR}$ is approximately 70%; approximately 4-nm WBR is present at approximately 26vol%; and the SH is χ~0.208.

4. Discussions

Ichitsubo *et al.* [21] demonstrate that SH is related to *m*, which represents the temperature dependence of supercooled liquids. Figure 4 shows the relationship between χ and *m* for ZC, ZCA, ZCNA, PNP, and PNCP MGs. For the Zr-based MGs, it shows that as χ increases, *m* decreases. For the Pd-based MGs, it shows the same tendency. However, regarding the diversification of constituent elements in the Zr- and Pd-based MGs, an inverse correlation between *m* and χ exists owing to differences in the types of constituent atoms and the manner of bonding. For example, a relatively wide-ranging network is generated by various types of strong chemical bonds centered on Zr in the case of the Zr-based MGs, whereas a relatively weak network is generated by Pd–Cu–P and Pd–Ni–P atomic pairs, which form cluster-like local structures in the case of the Pd-based MGs [31,32]

Lewandowsiki *et al.* [33] show that the intrinsic plasticity or brittleness of MGs correlates with their Poisson's ratio (*v*), that is, as *v* increases, the ductility of the MGs is improved. In addition, the elastic moduli are important parameters for understanding the correlation between structural characteristics and relevant mechanical properties. Thus, χ is also compared with *v*. Figure 5 shows the relationship between χ and *v* for ZC, ZCA, ZCNA, PNP, and PNCP MGs. For the Zr-based MGs, as χ increases, *v* increases. For the Pd-based MGs, the same tendency is observed. Regarding the correlation with *v*, the same trend is observed for both Zr- and Pd-based MGs. However, the diversification of constituent elements has an inverse correlation with χ, *m*, and *v* in the Zr- and Pd-based MGs. This can be considered to be influenced by the type of atoms constituting the alloy and the manner in which the atoms are bonded (metallic bonds, covalent bonds, etc.).

5. Conclusions

In this study, the SH of three types of Zr-based MGs and two types of Pd-based MGs is investigated using a dynamic viscoelastic model. Thereafter, the SH is evaluated using $\chi = VE_{c,WBR}/VE_{c,total}$.

1. ZCNA: $E_{c,WBR}/E_{c,SBR}$ is approximately 87%; approximately a 1-nm WBR is present at approximately 28vol%; and the SH is χ~0.241.

2. PNCP: $E_{c,WBR}/E_{c,SBR}$ is approximately 70%; approximately 4-nm WBR is present at approximately 26vol%; and the SH is χ~0.208.
3. A comparison of χ, m, and v show that as χ increased, m decreased and v increased. Moreover, the diversification of constituent elements is inversely related to χ, m, and v in the Zr- and Pd-based MGs.

Reference

1. W.H. Wang, Prog. Mater. Sci. **106**, 100561 (2019) https://doi.org/10.1016/j.pmatsci.2019.03.006
2. W.H. Wang, Prog. Mater. Sci. **57**, 487-656 (2012) https://doi.org/10.1016/j.pmatsci.2011.07.001
3. K. Tao, J.C. Qiao, Q.F. He, K.K. Song, Y. Yang, Int. J. Mech. Sci. **201**, 106469 (2021) https://doi.org/10.1016/j.ijmecsci.2021.106469
4. L.T. Zhang, Y.J. Wang, E. Pineda, Y. Yang, J.C. Qiao, Int. J. Plast. **157**, 103402 (2022) https://doi.org/10.1016/j.ijplas.2022.103402
5. H. Kato., T. Ichitsubo, H. Wang, T. Wada, J. Jpn. Soc. Powder Powder Metal. **60**, 228-235 (2013) https://doi.org/10.2497/jjspm.60.228
6. H. Wang, T. Ichitsubo, H. Kato, Eur. Phys. J. Appl. Phys. 98, 8 (2023) https://doi.org/10.1051/epjap/2022220266
7. H. Zhang, X. Wang, H.-B. Yu, J.F. Douglas, J. Chem. Phys. **154**, 084505 (2021) https://doi.org/10.1063/5.0039162
8. L. Hu, Y. Yue, J. Phys. Chem. C **113**, 15001-15006 (2009) https://doi.org/10.1021/jp903777f
9. H.B. Yu, X. Shen, Z. Wang, L. Gu, W.H. Wang, H.Y. Bai, Phys. Rev. Lett. **108**, 015504 (2012) https://doi.org/10.1103/PhysRevLett.108.015504
10. H.B. Yu, W.H. Wang, H.Y. Bai, Y. Wu, M.W. Chen, Phys. Rev. B **81**, 220201 (2010) https://doi.org/10.1103/PhysRevB.81.220201
11. S. Bhattacharya, R. Suryanarayanan, J. Pharm. Sci. **98**, 2935-2953 (2009) https://doi.org/10.1002/jps.21728
12. H. Tanaka, Phys. Rev. E **69**, 021502 (2004) https://doi.org/10.1103/PhysRevE.69.021502
13. G.P. Johari, M. Goldstein, J. Chem. Phys. **53**, 2372–88 (1970) https://doi.org/10.1063/1.1674335
14. R. Casalini, C.M. Roland, Phys. Rev. Lett. **102**, 035701 (2009) https://doi.org/10.1103/PhysRevLett.102.035701
15. G.P. Johari, J. Non-Cryst. Solids **307–310**, 317–25 (2002) https://doi.org/10.1016/S0022-3093(02)01491-6
16. Z. Lu, B.S. Shang, Y.T. Sun, Z.G. Zhu, P.F. Guan, W.H. Wang, H.Y. Bai, J. Chem. Phys. **144**, 144501, (2016) https://doi.org/10.1063/1.4945279
17. K.L. Ngai, S. Capaccioli, Phys. Rev. E **69**, 031501 (2004) https://doi.org/10.1103/PhysRevE.69.031501

18. D.P. Wang, J.C. Qiao, C.T. Liu, Materials Research Letters **7**, 305–11 (2019) https://doi.org/10.1080/21663831.2019.1604441
19. H.B. Yu, K. Samwer, Y. Wu, W.H. Wang, Phys. Rev. Lett. **109**, 095508 (2012) https://doi.org/10.1103/PhysRevLett.109.095508
20. F. Zhu, H.K. Nguyen, S.X. Song, D.P.B. Aji, A. Hirata, H. Wang, K. Nakajima, M.W. Chen, Nature Communications **7**, 11516 (2016) https://doi.org/10.1038/ncomms11516
21. T. Ichitsubo, H. Kato, E. Matsubara, S. Biwa, S. Hosokawa, K. Mats, H. Uchiyama, A.Q.R. Baron, J. Non-Cryst. Solids **357**, 494-500 (2011) https://doi.org/10.1016/j.jnoncrysol.2010.06.056
22. J.C. Qiao, H. Wang, J.M. Pelletier, H. Kato, Mater. Sci. Eng. A **600**, 32-36 (2014) https://doi.org/10.1016/j.msea.2014.02.007
23. J.Z. Jiang, K. Saksl, N. Nishiyama, A. Inoue, J. Appl. Phys. **92**, 3651-3656 (2002) https://doi.org/10.1063/1.1505681
24. W.H. Wang, J.J. Lewandowski, A.L. Greer, J. Mater. Res. **20**, 2307-2313 (2005) https://doi.org/10.1557/jmr.2005.0302
25. S. Zhang, T. Ichitsubo, E. Matsubara, Y. Yokoyama, T. Yamamoto, J. Mater. Sci., Jpn., **58**, 205–208 (2009) https://doi.org/10.2472/jsms.58.205
26. O. Haruyama, Y. Nakayama, R. Wada, H. Tokunaga, J. Okada, T. Ishikawa, Y. Yokoyama, Acta Mater. **58**(5), 1829-1836 (2010) https://doi.org/10.2320/matertrans.ME200825
27. Japan Institute of Metals, Metal Data Book, 4th ed. (Maruzen, Sendai, 2004)
28. H.S. Chen, J. Non-crst. Solids, **46**(3), 289-305 (1981) https://doi.org/10.1016/0022-3093(81)90007-7
29. J.Q. Qiao, R. Casalini, J.M. Pelletier, H. Kato, J. Phys. Chem. B **118**(13), 3720-3730 (2014) https://doi.org/10.1021/jp4121782
30. K.L. Ngai, M. Paluch, J. Chem. Phys. **120**, 857-873 (2004) https://doi.org/10.1063/1.1630295
31. Y. Takahara, N. Narita, Mater. Trans. **45**, 1172-1176 (2004) https://doi.org/10.2320/matertrans.45.1172
32. O. Gross, N. Neuber, A. Kuball, B. Bochtler, S. Hechler, M. Frey, R. Busch, Commun. Phys. **2**, 83 (2019) https://doi.org/10.1038/s42005-019-0180-2
32. Lewandowski * J. J., Wang W. H., Greer A. L., *Philosophical Magazine Letters*, **85**, 77–87 (2005) https://doi.org/10.1080/09500830500080474

33. K.K. Song, P. Gargarella, S. Pauly, G.Z. Ma, U. Kühn, J. Eckert, J. Appl. Phys. **112**, 063503 (2012) https://doi.org/10.1063/1.4752263
34. L. Battezzati L., Mater. Trans. **46**, 2915-2919 (2005) https://doi.org/10.2320/matertrans.46.2915
35. L. Xia, K.C. Chan, S.K. Kwok, P. Yu, J. *Non*-Cryst. *Solids*, **357**, 1469-1472 (2011) https://doi.org/10.1016/j.jnoncrysol.2010.12.040
36. Z. Zhang, V. Keppens, P.K. Liaw, Y. Yokoyama, A. Inoue, J. Mater. Res. **22**, 364-367 (2007) https://doi.org/10.1557/jmr.2007.0040
37. M. Jiang, L. Dai, Phys. Rev. B **76**, 054204 (2007) https://doi.org/10.1103/PhysRevB.76.054204
38. T. Rouxel, J. Chem. Phys. **135**, 184501 (2011) https://doi.org/10.1063/1.3656695

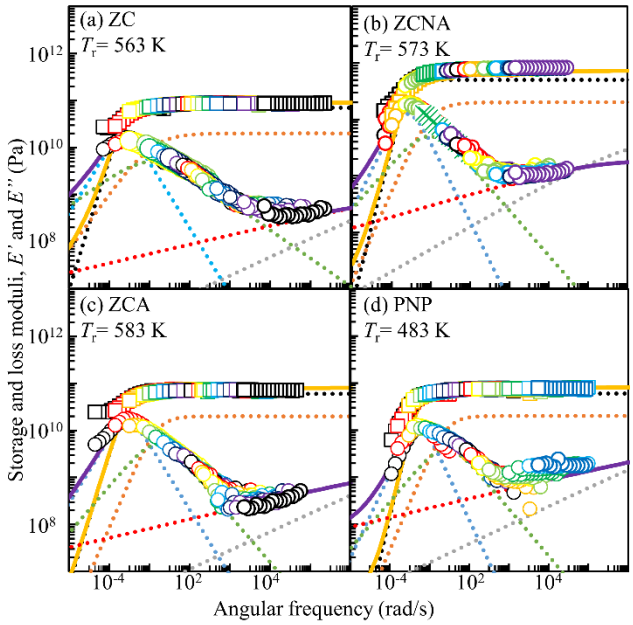

Figure 1. Isothermal frequency dispersion of elastic moduli for (a) $Zr_{50}Cu_{50}$ (ZC), (b) $Zr_{50}Cu_{40}Al_{10}$ (ZCA), (c) $Zr_{55}Cu_{30}Ni_5Al_{10}$ (ZCNA), and (d) $Pd_{40}Ni_{40}P_{20}$ (PNP) MGs; □ and ○ are measured E' and E'', respectively; —, —, ••, ••, ••, ••, ••, and •• are calculated E', E'', E'_{α}, E''_{α}, $E'_{s\beta}$, $E''_{s\beta}$, $E'_{f\beta}$, and $E''_{f\beta}$, respectively.

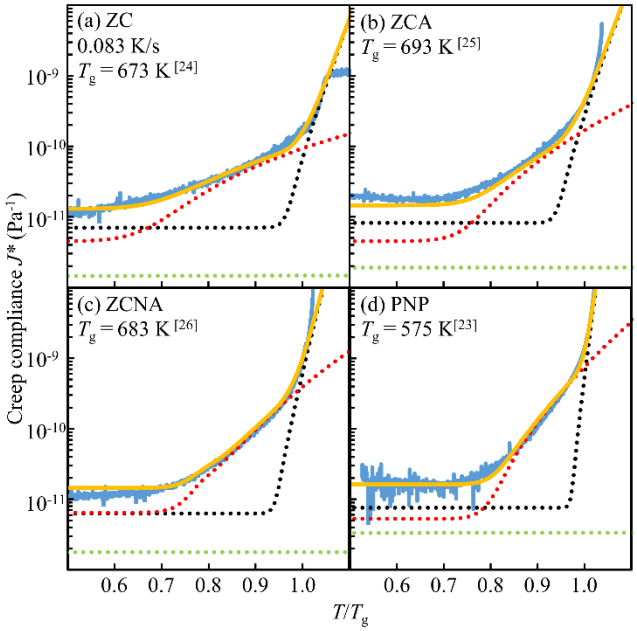

Figure 2. Isochronal temperature dispersion of tensile creep compliance for (a) $Zr_{50}Cu_{50}$ (ZC), (b) $Zr_{50}Cu_{40}Al_{10}$ (ZCA), (c) $Zr_{55}Cu_{30}Ni_5Al_{10}$ (ZCNA), and (d) $Pd_{40}Ni_{40}P_{20}$ (PNP) MGs; —,—, ••, ••, and •• are measured J^*, J^*_{total}, J^*_{α}, $J^*_{s\beta}$, and $J^*_{f\beta}$, respectively.

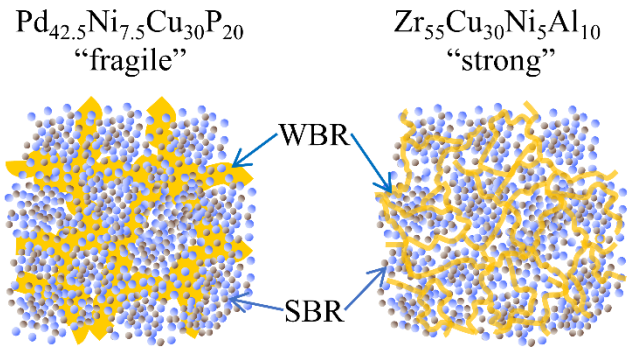

v_{WBR}~ 26vol%
ξ_{WBR}~ 4 nm
$E_{c,WBR}/E_{c,SBR}$~ 70%
χ~ 0.208

v_{WBR}~ 28vol%
ξ_{WBR}~ 1 nm
$E_{c,WBR}/E_{c,SBR}$~ 87%
χ ~ 0.241

Figure 3. Schematic of structural characteristics of Zr- and Pd-based MGs.

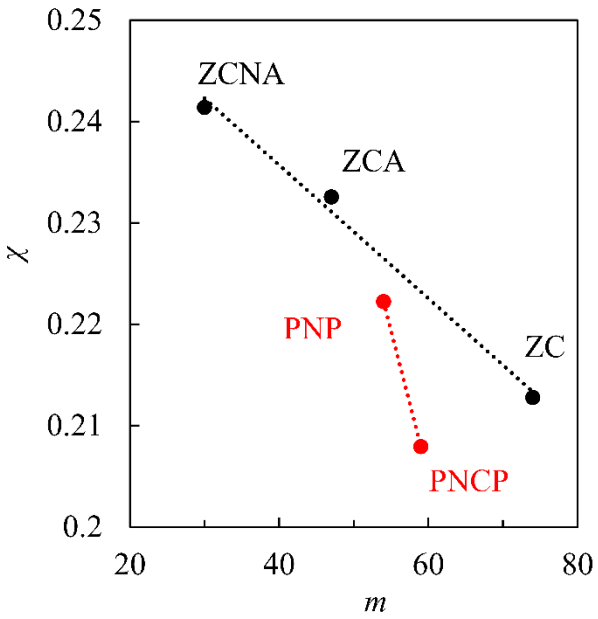

Figure 4. Relationship between χ and m for $Zr_{50}Cu_{50}$ (ZC), $Zr_{50}Cu_{40}Al_{10}$ (ZCA), $Zr_{55}Cu_{30}Ni_5Al_{10}$ (ZCNA), $Pd_{40}Ni_{40}P_{20}$ (PNP), and $Pd_{42.5}Ni_{7.5}Cu_{30}P_{20}$ (PNCP) MGs

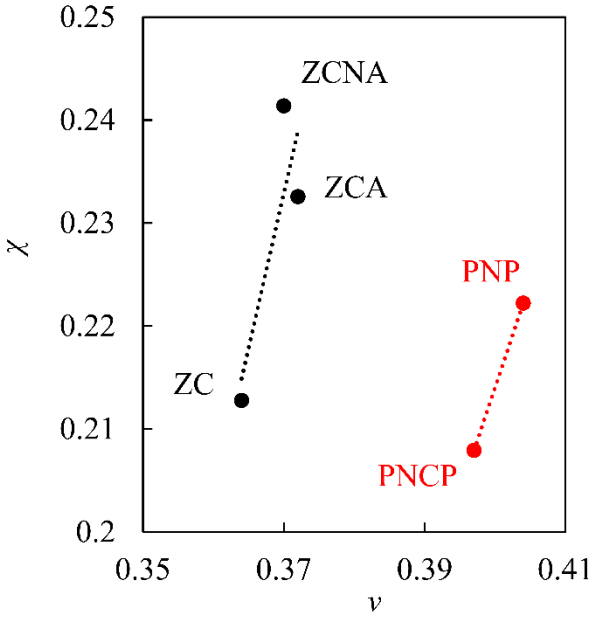

Figure 5. Relationship between χ and v for $Zr_{50}Cu_{50}$ (ZC), $Zr_{50}Cu_{40}Al_{10}$ (ZCA), $Zr_{55}Cu_{30}Ni_5Al_{10}$ (ZCNA), $Pd_{40}Ni_{40}P_{20}$ (PNP), and $Pd_{42.5}Ni_{7.5}Cu_{30}P_{20}$ (PNCP) MGs.

Table 1. Fitting parameters (Q, ω_0, β_{KWW}, and VE_c) obtained from dynamic viscoelastic model for isothermal dynamic mechanical analysis on $Zr_{50}Cu_{50}$ (ZC), $Zr_{50}Cu_{40}Al_{10}$ (ZCA), $Zr_{55}Cu_{30}Ni_5Al_{10}$ (ZCNA), $Pd_{40}Ni_{40}P_{20}$ (PNP), and $Pd_{42.5}Ni_{7.5}Cu_{30}P_{20}$(PNCP) metallic glasses; Q, ω_0, β_{KWW}, and VE_c are activation energy, pre-exponential factor, Korausch-Williams-Watts (KWW) stretched exponent, and relaxation intensity, respectively.

		Q	ω_0	β_{KWW}	VE_c
		eV	rad/s		GPa
ZC	α	2.9	5.5×10^{22}	0.7	70
	sβ	1.2	7.6×10^{8}	0.3	20
	fβ	(0.6)	(10^{14})	(0.1)	(4)
ZCA	α	3.3	2.7×10^{25}	0.9	60
	sβ	1.5	2.2×10^{11}	0.5	20
	fβ	(0.6)	(10^{14})	(0.1)	(6)
ZCNA	α	5.1	5.1×10^{41}	0.7	60
	sβ	1.6	1.1×10^{12}	0.4	20
	fβ	(0.6)	(10^{14})	(0.1)	(7)
PNP	α	5.92	1.7×10^{59}	0.8	50
	sβ	1.6	3.5×10^{15}	0.5	20

	fβ	(0.5)	(1.0×10^{14})	(0.13)	(10)
PNCP[5]	α	7.98	5.05×10^{68}	0.64	71
	sβ	1.39	1.0×10^{14}	0.38	18
	fβ	0.25	1.0×10^{14}	0.21	22

Table 2. Fitting parameters (Q, β_{KWW}, VE_c, V, and E_c) obtained from dynamic viscoelastic model for isochronal creep compliance on $Zr_{50}Cu_{50}$ (ZC), $Zr_{50}Cu_{40}Al_{10}$ (ZCA), $Zr_{55}Cu_{30}Ni_5Al_{10}$ (ZCNA), $Pd_{40}Ni_{40}P_{20}$ (PNP), and $Pd_{42.5}Ni_{7.5}Cu_{30}P_{20}$ (PNCP) metallic glasses; Q, β_{KWW}, VE_c, V, and E_c are activation energy, Korausch-Williams-Watts (KWW) stretched exponent, relaxation intensity, volume fraction, and characteristic elastic moduli, respectively; χ, m, and v are degrees of structural heterogeneity derived from $VE_{c,WBR}/VE_{c,total}$, fragility, and Poisson ratio, respectively.

		Q	β_{KWW}	VE_c	V	E_c	χ	m	v
		eV		GPa		GPa			
ZC	α	3.2	0.9	70	0.71	98	0.213	74[33]	0.364[34]
	sβ	1	0.3	20	0.29	70			
	fβ	(0.4)	(0.01)	(4)	-	-			
ZCA	α	3.2	0.9	60	0.7	86	0.233	47[35]	0.372[36]
	sβ	1.1	0.5	20	0.3	67			
	fβ	(0.4)	(0.01)	(6)	-	-			
ZCNA	α	5.6	0.9	60	0.72	84	0.241	30[37]	0.370[36]
	sβ	1.5	0.3	20	0.28	73			
	fβ	(0.4)	(0.01)	(6)	-	-			
PNP	α	6.8	0.9	60	0.68	89	0.222	54[38]	0.404[34]
	sβ	1.6	0.5	20	0.33	62			
	fβ	(0.4)	(0.01)	(10)	-	-			
PNCP[6]	α	7.65	0.9	78	0.74	105	0.208	59[38]	0.397[34]
	sβ	1.38	0.65	21	0.26	84			
	fβ	0.25	0.02	2	-	-			